



1 **Elevational Dependence of Global Forest Fires and Associated Aerosol Optical**
2 **Depth: Drivers and Decoupling**

3 Qiaomin Pei ¹, Chuanfeng Zhao ^{1,2,*}, Xing Yan ^{3,4}, Xingchuan Yang ⁵, Annan Chen ¹, Xin Wan ⁶

4 1 *Department of Atmospheric and Oceanic Sciences, School of Physics, Peking University, Beijing*
5 100871, China.

6 2 *Institute of Carbon Neutrality, Peking University, Beijing 100871, China.*

7 3 *State Key Laboratory of Earth Surface Processes and Disaster Risk Reduction, Faculty of*
8 *Geographical Science, Beijing Normal University, Beijing 100875, China*

9 4 *Advanced Interdisciplinary Institute of Satellite Applications, Faculty of Geographical*
10 *Science, Beijing Normal University, Beijing 100875, China*

11 5 *College of Resource Environment and Tourism, Capital Normal University, Beijing 100048, China*

12 6 *State Key Laboratory of Tibetan Plateau Earth System, Resources and Environment (TPESRE),*
13 *Institute of Tibetan Plateau Research, Chinese Academy of Sciences, Beijing 100101, China*

14

15 Correspondence to: Chuanfeng Zhao (cfzhao@pku.edu.cn)

16



17 **Abstract**

18 Forest fires have become an escalating environmental and ecological issue
19 worldwide over the past decades. However, a knowledge gap persists in globally
20 assessing how topography modulates wildfire behavior. Here we quantify global
21 spatiotemporal patterns of forest fire activity and associated aerosol optical depth
22 (AOD), together with elevation-dependent controls, using satellite observations from
23 2012 to 2024. The analysis reveals a slight yet significant increase in fire occurrence,
24 accompanied by a strong positive association with fine-mode AOD (FAOD). In contrast,
25 coarse-mode AOD (CAOD) shows little response, implying that wildfire emissions
26 mainly contribute to the fine aerosol fraction. Forest fire occurrence declines
27 systematically with elevation, with most fires concentrated below 600 m. In contrast,
28 FAOD exhibits elevated mean values and increasing trends at mid-elevations (600–
29 1400 m), revealing a decoupling between fire frequency and aerosol loading. This
30 divergence is consistent with shifts in forest-type composition and topographically
31 modulated smoke transport, including aerosol self-lifting driven by radiative absorption
32 and atmospheric convection. Elevation-stratified multiple linear regression analyses
33 incorporating the Fire Weather Index, leaf area index, temperature, wind speed, and
34 precipitation indicate that fire activity is primarily governed by fuel availability and
35 aridity. Precipitation exerts a consistent suppressive effect across elevations, while wind
36 speed enhances fuel drying and fire spread at mid-elevations. Overall, these results
37 identify elevation as a key organizing factor linking forest fires, aerosol emissions, and
38 their underlying drivers, providing new constraints for wildfire risk assessment and
39 fire–aerosol interactions under a changing climate.

40



411. **Introduction**

42 Wildfires represent a key component of the Earth system, influencing ecosystems,
43 atmospheric composition, carbon cycling, climate, and public health on a global scale
44 (Bowman et al., 2009; Andela et al., 2017; Qian, 2025; Yang et al., 2022; Yang et al.,
45 2021a). Over the past decade, the societal and environmental consequences of wildfires
46 have attracted increasing scientific and public attention (Abatzoglou et al., 2025).
47 Concurrently, ongoing climate warming has intensified fire-conducive weather,
48 increasing the probability of wildfire occurrence, particularly large and extreme events
49 (Jones et al., 2024; Abatzoglou et al., 2025). Elevated temperatures and prolonged
50 dryness further reduce fuel moisture, raising fire susceptibility in biomass-rich forests
51 (Jones et al., 2024; Jolly et al., 2015).

52 Forests constitute the most extensive terrestrial biome and serve as a major
53 component of the global carbon budget (Pan et al., 2011). Despite their critical role,
54 these ecosystems are becoming increasingly vulnerable to wildfire disturbances
55 (Keywood et al., 2013). While the total burned area worldwide has shown a declining
56 tendency in recent decades, fire occurring in forested regions have become more
57 frequent and more severe, with average fire size, duration, and intensity increasing by
58 two- to threefold over recent decades (Zheng et al., 2021; Cunningham et al., 2024;
59 Parisien et al., 2023; Canadell et al., 2021). Escalating occurrences of extreme fires
60 threaten forest stability and recovery capacity, potentially undermining essential
61 ecosystem functions and services, including long-term carbon storage (Ward et al.,
62 2020; Gatti et al., 2021). In contrast to grasslands, forest fires release greater amounts
63 of carbon dioxide per unit area, and the reestablishment of carbon sinks after burning
64 is generally slow, which may generate a positive climate-fire feedback (Zheng et al.,
65 2021). These risks are further intensified by climate change, which promotes fuel aridity,
66 extreme fire weather, and longer fire seasons, thereby increasing the probability of
67 large-scale biomass burning (Kirchmeier-Young et al., 2024; Wang et al., 2025). Large
68 and extreme fires are also promoted by human disturbance and land-use change,
69 particularly in tropical forests where frequent human ignitions and ongoing forest



70 degradation strongly drive fire activity (Lapola et al., 2023; Yang et al., 2023). By
71 completely or partially removing aboveground vegetation, wildfires fundamentally
72 alter forest structure and function (Kim et al., 2025), making forest fire activity an
73 increasingly urgent global environmental and ecological concern.

74 The combustion of biomass in forest fires releases significant quantities of
75 aerosols and trace gases into the atmosphere, leading to pronounced air quality
76 deterioration not only near source regions but also in distant areas affected by long-
77 range smoke transport (Ma et al., 2025; Zhang et al., 2025; Fan et al., 2021; Xu et al.,
78 2025). Smoke-related pollution markedly increases annual mean PM_{2.5} exposure,
79 contributing to thousands of premature deaths and billions of U.S. dollars in economic
80 losses each year (Ma et al., 2025; Zhang et al., 2025). In addition to these air quality
81 impacts, smoke aerosols influence the Earth's radiation balance and climate system
82 through both direct interactions with solar radiation (scattering and absorption) and
83 indirect effects associated with cloud microphysics (Keywood et al., 2013; Andreae et
84 al., 2004; Blanchard-Wrigglesworth et al., 2025). Wildfire emissions induce contrasting
85 thermal effects, characterized by surface cooling and atmospheric warming, which
86 modify atmospheric stability, vertical transport, circulation patterns, and regional
87 hydrology, ultimately driving significant climatic responses (Menon et al., 2002; Koren
88 et al., 2004; Lau et al., 2006; Blanchard-Wrigglesworth et al., 2025; Pei et al., 2025).
89 Moreover, wildfire-derived aerosols affect atmospheric and oceanic biogeochemistry
90 by modulating nutrient deposition and photosynthetic activity in marine ecosystems
91 (Hamilton et al., 2022; Tang et al., 2021). Consequently, wildfire emissions exert broad
92 effects on air quality, the global radiation balance, and coupled climate–biogeochemical
93 systems.

94 Substantial studies have elucidated that vegetation cover, fire weather, climate and
95 topography jointly govern the probability and severity of forest fires (Parks et al., 2018;
96 Birch et al., 2015; Whitman et al., 2018; Wang et al., 2022c; Yu et al., 2020). Besides
97 fire weather and climate forcing, vegetation characteristics and topographic controls are
98 critical determinants of fire severity, particularly in mountainous terrain (Birch et al.,



99 2015; Walker et al., 2020). Live fuel availability, represented by vegetation cover, has
100 been shown to strongly regulate wildfire severity. Analyses of 19 forested ecoregions
101 across the western United States for 2002–2015 highlighted it as the dominant control
102 (Parks et al., 2018), with comparable relationships documented in both the northern
103 Rocky Mountains (Birch et al., 2015) and North American boreal forests (Walker et al.,
104 2020; Whitman et al., 2018). Using a machine-learning approach, Jones et al. (2024)
105 categorized global forest ecoregions into 12 pyromes and showed that increases in
106 forest cover and ecosystem productivity substantially enhanced wildfire emissions.
107 Topographic factors—such as elevation, aspect, and slope—have also been shown to
108 exert substantial influence on burn severity across diverse regions, including China and
109 Canada (Huang et al., 2020; Whitman et al., 2018). Notably, investigations from the
110 Canadian Rocky Mountains reported strong associations between elevation and fire
111 activity (Rogean and Armstrong, 2017). Despite these advances, global-scale
112 assessments of the relationship between topography and fire regimes remain limited
113 relative to the extensive focus on vegetation-related drivers. This gap is notable given
114 that topography can substantially enhance fire spread and promote erratic fire behavior
115 (Sharpley et al., 2012).

116 This work examines the influence of topography on global forest fire activity
117 through a comprehensive analysis of spatial fire patterns. Building on evidence from
118 Canadian forests identifying elevation as a key topographic control (Wang et al., 2025),
119 we focus on elevation as a central organizing factor. This study focuses on three main
120 objectives: (i) describing the global spatial distribution of fire pixel counts and their
121 associations with aerosol optical depth (AOD) over forested regions; (ii) assessing the
122 extent to which elevation shapes the spatial patterns of both fires and AOD; and (iii)
123 determining the key factors that control the elevation–fire relationship. To interpret
124 these patterns, multiple explanatory variables, including fuel load, forest type, and fire
125 weather, are jointly analyzed. By elucidating elevation-dependent fire dynamics, this
126 work provides a scientific basis for adaptive fire management, elevation-informed fuel
127 treatments, post-fire hazard mitigation, and ecologically informed fire use to support



128 biodiversity conservation in the face of persistent climate warming.

129 **2. Materials and methods**

130 **2.1 Satellite-based wildfire observations**

131 We utilized active fire observations from the Visible Infrared Imaging Radiometer
132 Suite (VIIRS) sensors carried by the Suomi NPP and NOAA-20 platforms. These
133 measurements capture combustion-related thermal signals at approximately 375 m
134 resolution. To facilitate large-scale analysis, individual fire detections were spatially
135 aggregated onto a $0.1^\circ \times 0.1^\circ$ global grid, and the number of detections within each cell
136 was used as a metric of fire occurrence. Daily wildfire activity was characterized using
137 the combined daytime and nighttime VIIRS observations, accounting for both fire
138 occurrence and intensity. Fire detections were spatially overlaid with a forest land-cover
139 mask to extract events occurring within forested pixels, and only grid cells with more
140 than one active fire detection during 2012–2024 were retained to ensure data robustness.
141 To enhance data reliability, fire pixels flagged as “low confidence” (confidence level
142 ‘1’) were excluded from the analysis.

143 **2.2 Vegetation types, elevation, and fire weather data**

144 Land cover information was characterized by using the MODIS land cover type
145 dataset at 500 m resolution, available through NASA’s Land Processes Distributed
146 Active Archive Center (LP DAAC). Topographic characteristics were represented using
147 the General Bathymetric Chart of the Oceans (GEBCO) 2024 gridded data, which
148 provides global elevation and bathymetry data at 15-arc-second resolution (~500 m)
149 (Harper and Sandwell, 2024). To ensure spatial consistency, land cover and elevation
150 datasets were resampled to match the analysis grid. Forest categories and elevation
151 values at fire locations were then extracted using nearest-neighbor interpolation.
152 Forested regions were grouped into five major types: evergreen needleleaf (ENF),
153 evergreen broadleaf (EBF), deciduous needleleaf (DNF), deciduous broadleaf (DBF),
154 and mixed forest (MF). Elevation was stratified into 20 zones using 100 m intervals
155 below 2000 m. Given the relatively low number of fire detections at higher elevations,
156 all regions above 2000 m were combined into a single category to ensure sufficient



157 sample sizes and enhance the robustness of subsequent trend analyses.

158 We employed the Canadian Forest Fire Weather Index (FWI) system to
159 characterize weather conditions that favor wildfire development and to assess climate-
160 driven variability in fire danger (Su et al., 2025; Liu et al., 2023; Van Wagner, 1987).
161 The index is calculated from standard meteorological inputs, including near-surface air
162 temperature, wind speed, relative humidity, and accumulated total precipitation over
163 the preceding 24-hour (Van Wagner, 1987). Daily FWI data with a resolution of 0.25°
164 $\times 0.25^\circ$ from 2012 to 2024 are obtained from the historical fire danger index archives.
165 Supplementary meteorological parameters, such as 2 m air temperature (2mT), 10 m
166 wind speed (10mW), and the max daily total precipitation, were extracted from the
167 ERA5 reanalysis produced by the European Centre for Medium-Range Weather
168 Forecasts (ECMWF). Monthly means of FWI and meteorological variables were
169 calculated for subsequent analyses with forest fire activity.

170 **2.3 Satellite-based FAOD and CAOD retrievals**

171 Size-resolved aerosol optical depths at 500 nm, including the fine (FAOD) and
172 coarse (CAOD) fractions, were estimated using SIDN (Simultaneous FAOD–CAOD
173 Inversion Deep Neural Network) algorithm. The inversion is physically constrained by
174 incorporating interactions between the two aerosol size classes, thereby enhancing
175 retrieval reliability (Luo et al., 2024; Chen et al., 2025). SIDN integrates multi-source
176 satellite observations with meteorological reanalysis data and is trained against high-
177 quality AERONET measurements using a shared representation learning strategy based
178 on the EntityDenseNet architecture. By dynamically balancing FAOD and CAOD
179 contributions during training, SIDN improves retrieval accuracy and internal
180 consistency across diverse aerosol regimes. A comprehensive description of the model
181 architecture, training procedure, and validation is provided in the above references and
182 is not repeated here. Extensive evaluations against independent ground-based
183 observations demonstrate that SIDN outperforms conventional satellite products,
184 yielding reduced uncertainties and improved spatial completeness, particularly under
185 cloudy and complex surface conditions. The resulting daily global FAOD and CAOD



186 dataset spans 2012–2024 at a spatial resolution of 0.5° . A conservative nearest-neighbor
187 approach was applied to collocate gridded AOD fields with satellite-detected forest fire
188 locations.

189 **2.4 Temporal trends analysis**

190 Temporal trends in wildfire activity were assessed using linear regression applied
191 to annual fire pixel counts aggregated at $0.1^\circ \times 0.1^\circ$ resolution. For each grid cell, a
192 linear regression was fitted between the natural logarithm of annual fire pixel counts
193 and time, with statistical significance determined at $p < 0.05$. The regression slope was
194 exponentiated to estimate the annual percentage change in fire occurrence. For the
195 global and forest-type-specific assessments, annual records were further processed
196 with a 3-year centered moving average, which filters out short-term interannual noise.
197 To verify the stability of the detected trends, we employed the Mann–Kendall non-
198 parametric test in combination with the Theil–Sen estimator, which provide outlier-
199 insensitive assessments of trend direction and magnitude. The Theil–Sen slope was then
200 derived for grid cells showing significant changes, expressed as

$$201 \text{SFC} = \text{median} \left(\frac{FC_j - FC_i}{j - i} \right), 2012 \leq i < j \leq 2024$$

202 where SFC denotes the median rate of change, and FC_i and FC_j represent fire pixel
203 counts at moments i and j , respectively.

204 Trends in AOD over 2012–2024 were analyzed using the same logarithmic linear
205 regression framework to ensure comparability with fire pixel count trends. AOD values
206 were restricted to the range 0–5 to exclude extreme outliers.

207 **2.5 Correlation and multivariate regression analysis**

208 To quantify the influence of forest fires on aerosol loading, linear regressions of
209 the form $\text{AOD} = a + k \times \log_{10}[\text{fires}]$ applied separately to FAOD and CAOD. The
210 regression slope (k) represents fire sensitivity, with larger values indicating stronger
211 aerosol responses to fire activity. The $\log_{10}[\text{fires}]$ was adopted as the explanatory
212 variable, following common practice in wildfire research (Zhao et al., 2024; Abatzoglou
213 and Williams, 2016). We applied linear regressions to individual $2^\circ \times 2^\circ$ grid cells that



214 contained no fewer than 10 fire observations. Where statistically significant
215 associations were identified ($p < 0.05$), both the slope parameter (k) and the
216 corresponding R^2 values were mapped to illustrate their spatial variability. Differences
217 in regression slopes among grid cells were evaluated using two-tailed t tests.

218 For the elevation-based analysis of forest fire activity, all monthly fire,
219 meteorological, vegetation, and topographic variables were spatially resampled to a 1°
220 $\times 1^\circ$ grid. The finer resolution was adopted to retain sufficient grid-point samples within
221 elevation classes. For each grid cell, multiple linear regression model was conducted
222 with $\log_{10}[\text{fires}]$ as the response variable and FWI, leaf area index (LAI), 2mT, 10mW,
223 and daily maximum total precipitation as predictors. Year and month were additionally
224 included to represent long-term trends and seasonal variability. We employed ordinary
225 least squares (OLS) models to obtain baseline relationships, and statistical inference
226 was conducted using heteroskedasticity-robust standard errors ($p < 0.05$). To mitigate
227 multicollinearity among predictors, ridge regression with L_2 regularization was
228 additionally applied after standardizing all variables, with the optimal regularization
229 parameter selected via cross-validation. Variance inflation factors (VIFs) were
230 calculated to diagnose collinearity, and partial correlation analysis was applied to
231 isolate the independent effects of each driver after accounting for temporal influences.
232 Regression coefficients and model performance metrics were subsequently summarized
233 within elevation bins to characterize altitude-dependent fire–environment relationships.

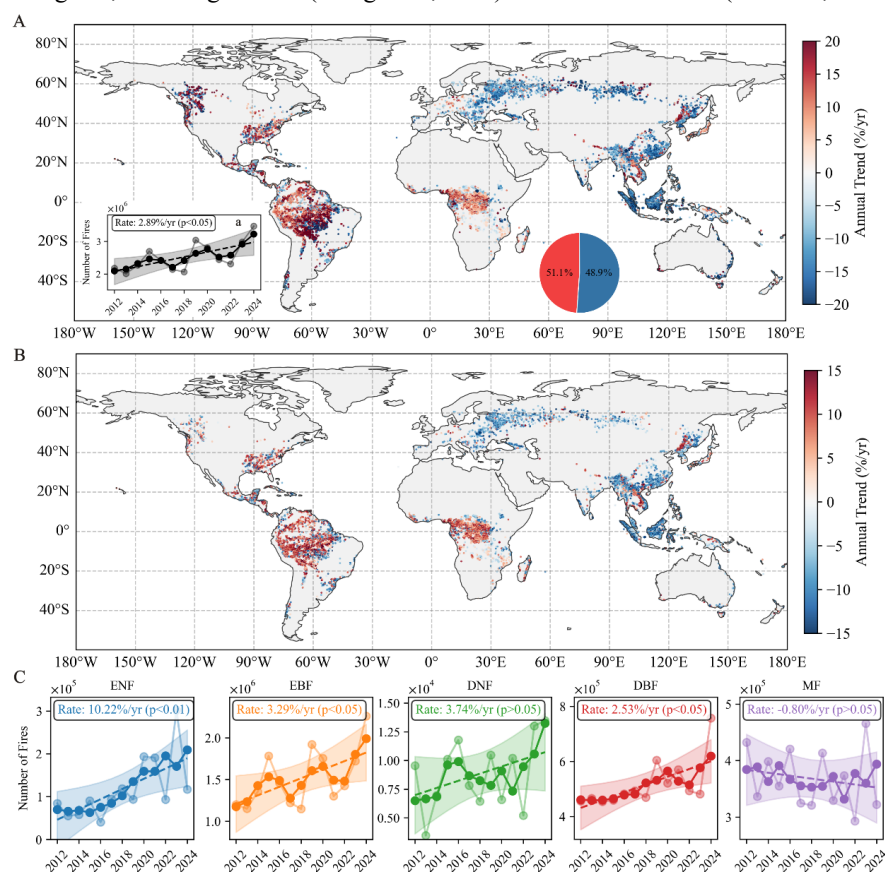
234 **3. Results and discussion**

235 **3.1 Spatiotemporal patterns of forest fires and AOD**

236 Analysis of satellite-derived fire pixel counts across global forested regions from
237 2012 to 2024 reveals a modest but statistically significant increasing trend. Spatially,
238 51.1% of forest grid cells exhibit positive trends, exceeding the 48.9% showing
239 negative trends, with a global mean linear increase of $2.89\% \text{ yr}^{-1}$ ($p < 0.05$, Figure 1A).
240 Our results indicate a growing number of forest fires, in agreement with the previously
241 reported global increase in forest burned area and mean fire pixel counts over last two
242 decades (Zheng et al., 2021; Yu and Ginoux, 2022). Geographically, significant positive



243 trends in fire pixel counts are concentrated in North America, northern South America,
244 and central Africa, whereas predominantly negative trends occur in Southeast Asia,
245 western and central Siberia, and eastern Europe (Figure 1A). The spatial patterns
246 derived from linear regression are consistent with those identified using the Mann-
247 Kendall test (Figure 1B). Notably, regions exhibiting increasing trends largely overlap
248 with areas of enhanced burned area and fire-driven carbon emissions in the tropical
249 moist broadleaf forest pyrome identified by Jones et al. (2024) for the period 2001–
250 2023. Increasing fire activity has also been reported in selected extratropical forest
251 ecoregions, including Canada (Wang et al., 2025) and Northeast China (Liu et al., 2023).

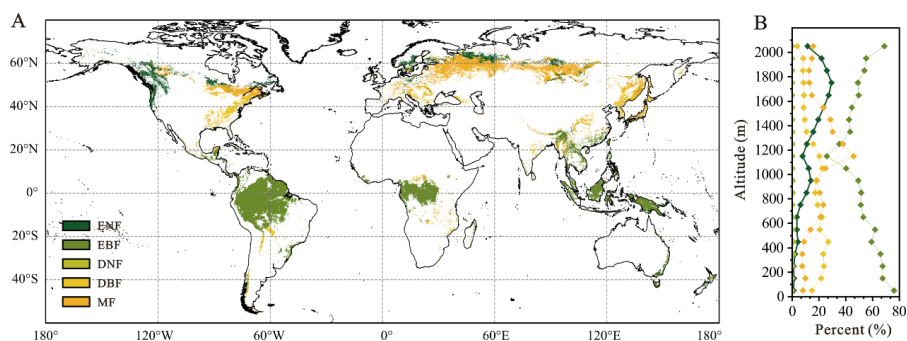


252
253 Figure 1. Global trends in forest fire occurrence during 2012–2024. (A) Spatial distribution of
254 statistically significant ($p < 0.05$) trends in annual fire pixel counts. The inset (a) shows the
255 corresponding global time series, including annual values (light circles), a 3-year centered moving



256 average (dark circles), and the fitted linear trend with its 95% confidence interval (dashed line and
257 shaded envelope). The accompanying pie chart summarizes the relative fractions of increasing (red)
258 and decreasing (blue) trends. (B) Significant spatial changes in yearly fire frequency, with
259 significance assessed by the Mann–Kendall test and slope magnitudes estimated using the Theil–
260 Sen method. (C) Distribution of significant interannual trends by dominant forest type, using the
261 same smoothing and trend analysis as in (a).

262 Considerable heterogeneity in fire activity is found across forest types. EBF
263 accounts for the largest proportion of fire pixel counts globally, whereas ENF exhibits
264 the strongest positive trend in fire occurrence (Figure 1C). By comparison, no
265 statistically significant changes are observed for DNF and MF. These forest types are
266 primarily distributed across western and central Siberia (Figure 2A), regions
267 characterized by declining fire activity (Figure 1A). Fire occurrence and severity are
268 strongly mediated by vegetation characteristics, including forest type and fuel structure
269 (Wang et al., 2025). High fire frequency and density are commonly associated with
270 evergreen needleleaf forests, such as those dominated by Chir pine (*Pinus roxburghii*),
271 which are characterized by high-intensity fire regimes (Kumar and Kumar, 2022). This
272 elevated fire susceptibility is attributed to needle-shaped foliage, high resin content, and
273 ladder-like branch architecture, which collectively enhance fuel flammability and
274 vertical fire spread (Alexander and Cruz, 2011; Wang et al., 2025).

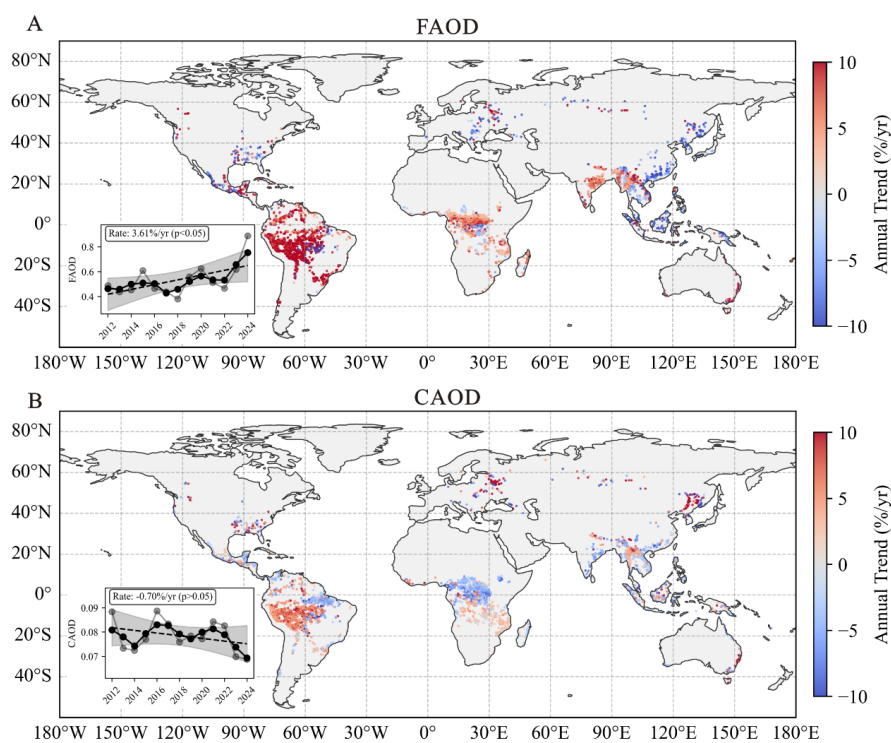


275
276 Figure 2. Forest classification and its topographic variation. (A) Spatial patterns of the dominant
277 forest categories. (B) Elevation-dependent distribution of forest cover, expressed as the percentage
278 area occupied by each type within individual elevation bands.

279 To examine aerosol responses to forest fire activity, aerosol loading was
280 characterized using FAOD and CAOD. A consistent positive association between



281 FAOD and fire pixel counts is observed across global forest regions from 2012 to 2024,
282 whereas no comparable trend is detected for CAOD (Figure 3). The fire–FAOD
283 relationship was quantified using linear regression of the form $(FAOD = a + k_F \times$
284 $\log_{10}[\text{fires}])$ applied to each $2^\circ \times 2^\circ$ grid cell. Widespread statistically significant
285 positive k_F values indicate that fine-mode particles dominate wildfire-related aerosol
286 loading (Figure 4A), consistent with previous evidence that biomass burning
287 predominantly contributes to the fine-mode portion of the aerosol population (Yan et
288 al., 2024; Yang et al., 2021b; Kaskaoutis et al., 2014; Pei et al., 2025).

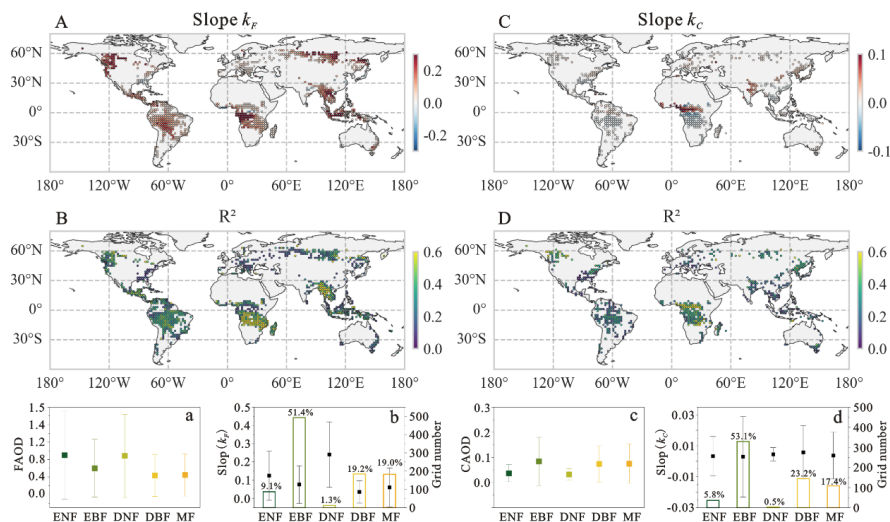


289
290 Figure 3. Spatiotemporal trends in FAOD and CAOD during 2012–2024. (A) Spatial distribution of
291 statistically significant trends ($p < 0.05$) in FAOD. (B) Corresponding distribution for CAOD. Insets
292 show the annual global time series, including annual values (light circles), a 3-year centered moving
293 average (dark circles), and the linear trend with its 95% confidence interval (dashed line with
294 shading).

295 The k_F slope values exhibited variation across forest types, with the highest values
296 magnitude observed in DNF (0.24 ± 0.18), followed by ENF (0.13 ± 0.13), EBF (0.08



297 ± 0.10), MF (0.06 ± 0.11) and DBF (0.04 ± 0.06) (Figure 4b). This ranking is consistent
 298 with the spatial pattern of average FAOD across these forest types (Figure 4a). Such
 299 differences can be attributed to species-dependent emission strengths, as dominant taxa
 300 contribute unevenly to wildfire-derived aerosols. For example, within ENF regions,
 301 *Pseudotsuga* and *Picea* account for 15% and 71.1% of total FAOD contribution from
 302 wildfire, respectively; among broadleaf forests, the genus *Quercus* alone contributes
 303 50.6% (Chen et al., 2025). These patterns underscore that aerosol emissions from forest
 304 fires depend not only on burned areas but also on fuel type and combustion efficiency
 305 (Keywood et al., 2013). In contrast, no significant positive k_C values are detected for
 306 CAOD (Figure 4C). The average of k_C values in different forest types was close to 0
 307 with minimal variation (Figure 4d), indicating the absence of a systematic forest fire
 308 influence on coarse-mode aerosol loading.



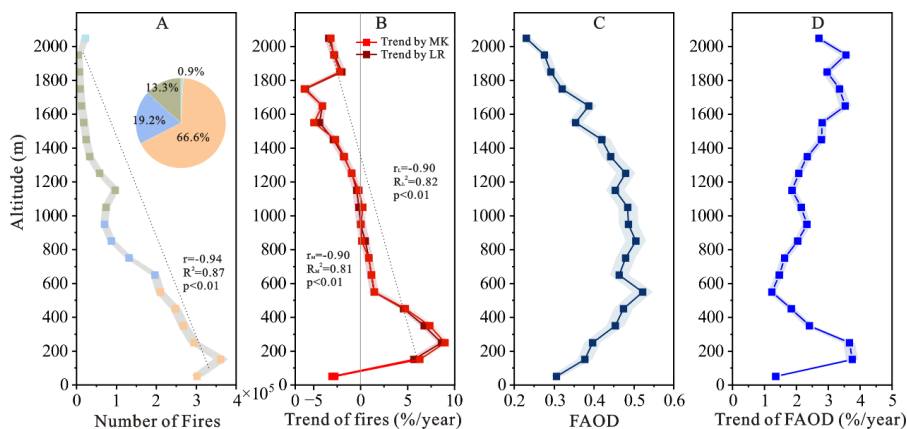
309 Figure 4. Correlation analysis between forest fires and AOD. (A, B) Regression slope k_F and R^2 for
 310 FAOD-fire relationship. (C, D) Slope k_C and R^2 for CAOD-fire relationship. (a, b) Forest-type
 311 averages of FAOD and Slope k_F . (c, d) Forest-type averages of CAOD and Slope k_C . Maps (A-D)
 312 show only locally significant relationships (linear regression, $p < 0.05$). Error bars in panels (a-d)
 313 denote standard errors. In panels (b) and (d), bar height indicates the number of grid cells per forest
 314 type, with numbers above bars showing the fractional area contribution of each forest type.

3.2 Elevation-Dependent Patterns of Forest Fire Occurrence and FAOD

317 To evaluate how topography shapes forest fire activity globally, we examined the



318 elevational dependence of fire occurrence from 2012 to 2024. A clear and statistically
 319 significant decline in mean annual fire pixel counts with increasing elevation was
 320 identified (Figure 5A). Forest fires were predominantly concentrated at low elevations,
 321 with 66.6% of total fire detections occurring below 600 m, followed by 19.2% between
 322 601 and 1000 m and 13.3% between 1001 and 2000 m. Only 0.9% of fires were detected
 323 above 2000 m (Figure 5A). This inverse relationship between elevation and fire activity
 324 agrees with previous regional studies conducted in the Canadian Rocky Mountains
 325 (Rogean and Armstrong, 2017) and across forested regions of China (Tian et al., 2013;
 326 Ma et al., 2020). Similar elevational dependence is also evident in the interannual trends.
 327 Both the multiyear mean fire pixel counts, and the corresponding annual trends exhibit
 328 a pronounced decrease from low to high elevations (Figure 5A, B). Notably, while the
 329 largest absolute number of fires were observed between 100 and 200 m, the strongest
 330 positive trend in fire activity occurred near ~300 m before declining at higher elevations.
 331 This discrepancy suggests that recent fire activity has increasingly concentrated around
 332 the ~300 m elevation range, potentially reflecting the combined influence of climate
 333 variability and fire management practices. In contrast, a weak negative trend in fire
 334 occurrence was observed below 100 m, which may be associated with more effective
 335 control of ignition sources in densely managed lowland regions (Wang et al., 2022b).



336
 337 Figure 5. Elevational variations in multiyear mean fire pixel counts, FAOD, and their temporal
 338 trends. (A, B) Multiyear mean (A) and significant annual trend (B) in fire pixel counts as a function
 339 of elevation. (C, D) Corresponding multiyear average (C) and trend (D) in FAOD. Dashed lines



340 indicate overall elevation-dependent tendencies in (A) and (B). Colors denote elevation classes: 0–
341 600 m (light orange), 600–1000 m (light blue), 1000–2000 m (gray-green), and >2000 m (light
342 cyan). Shaded areas represent the 95% confidence intervals.

343 In contrast to the monotonic decline in fire occurrence, FAOD exhibits a distinct
344 elevational pattern. While FAOD trends below 600 m broadly track those of fire activity,
345 its multiyear mean values peak at mid-elevations (600–1400 m) rather than at low
346 elevations (Figure 5C, D). This divergence indicates that FAOD is not solely controlled
347 by local fire occurrence but is also influenced by forest composition and
348 topographically modulated by smoke transport processes. Around 600 m elevation,
349 forest composition shifts toward a higher fraction of ENF (Figure 2B), which exhibits
350 stronger FAOD sensitivity to fire activity ($k_F = 0.13 \pm 0.10$) than EBF ($k_F = 0.08 \pm 0.10$).
351 In addition, smoke particles released by low-elevation fires may be carried to higher
352 levels of the atmosphere via aerosol self-lifting processes associated with radiative
353 heating and convective motions (De Laat et al., 2012; Ohneiser et al., 2023; Xu et al.,
354 2025), thus elevating FAOD levels at mid-elevations. Above 600 m, the strengthening
355 FAOD trends with elevation diverge from the concurrent decline in fire occurrence,
356 implying the involvement of additional processes beyond local fire emissions. In
357 addition, with fewer than 50 grid cells above 1500 m exhibiting statistically significant
358 trends, the representativeness and accuracy of the computed global FAOD trend may
359 be compromised. Collectively, these results suggest that mid-elevation regions (600–
360 1400 m) are disproportionately influenced by smoke aerosols from forest fires at a
361 global scale.

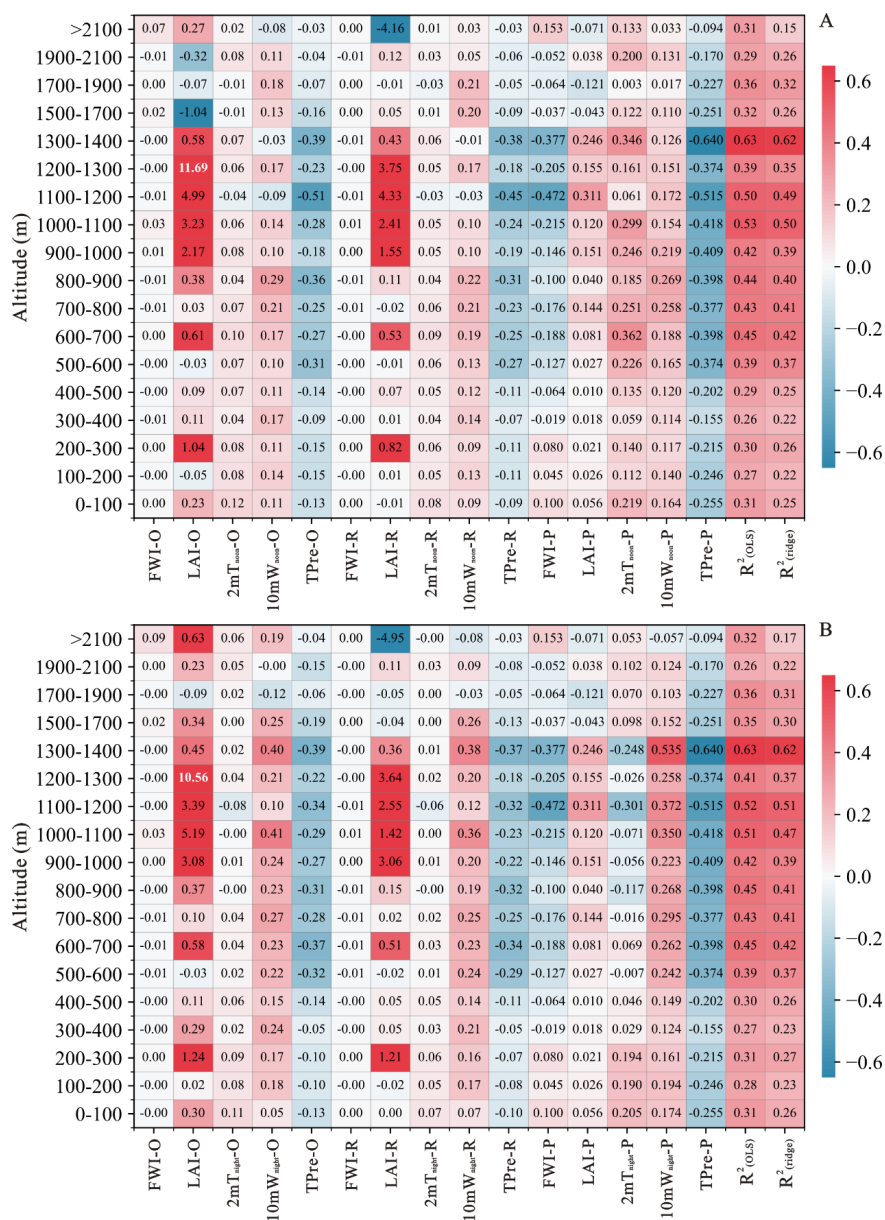
362 **3.3 Drivers of Elevational-Dependent Variations in Fire Activity**

363 To explain the contrasting elevational patterns of forest fire occurrence identified
364 in Section 3.2, we next examine the meteorological and ecological drivers governing
365 fire activity along with the elevation gradient. Vegetation fire activity is governed by
366 multiple interacting factors, including ignition sources, fuel supply and moisture, fire-
367 conducive weather, and forest management practices (Wang et al., 2022a; Clarke et al.,
368 2025). However, the relative contributions of these drivers change with elevation.
369 Notably, the FWI—often used to characterize short-term fire weather—exerts little



370 explanatory power, with regression coefficients near zero at all heights (Figure 6).
371 Partial correlation coefficients were negative between 300 and 2100 m, indicating a
372 weak association between FWI and fire occurrence after accounting for elevation. The
373 weak agreement observed here aligns with earlier reports (Su et al., 2025; Wang et al.,
374 2025) and arises primarily from mismatches in spatial and temporal resolution.
375 Specifically, FWI captures short-term meteorological extremes, our analysis focuses on
376 multiyear mean fire occurrence aggregated along elevation bands.

377 To further disentangle elevational controls on fire activity, we examined individual
378 climatic and ecological variables associated with fuel aridity, ignition potential, and fuel
379 availability. Observed declines in LAI and wind speed with increasing elevation (Figure
380 7) are consistent with a reduced probability of fire occurrence at higher altitudes. LAI
381 was selected as a proxy for fuel availability Yu et al. (2020). Multiple linear regression
382 analyses reveal pronounced elevation-dependent relationships (Figure 6). At high
383 elevations (>1500 m), fire occurrence shows no significant relationship with LAI. In
384 contrast, fire activity shows clear positive correlations with LAI at both low (200–300
385 m and 600–700 m) and mid-elevations (800–1400 m), highlighting the importance of
386 vegetation density as a proxy for available fuels. Although ridge regression produced
387 smaller coefficients than OLS, the coefficient for LAI remained significantly higher
388 than those of the other predictors. These observations support earlier studies showing
389 that vegetation structure and forest composition strongly regulate fire dynamics (Parks
390 et al., 2018; Wang et al., 2022c). In particular, evergreen needleleaf species such as
391 *Pinus densiflora* and *Pinus roxburghii* possess resin-rich needles that enhance
392 flammability and promote high-intensity fire behavior (Baek et al., 2022; Kumar and
393 Kumar, 2022).



394
 395 Figure 6. Elevational variations in the key drivers of fire activity derived from multiple linear
 396 regression. Fire pixel counts were related to the FWI, LAI, 2mT, 10mW, and maximum total
 397 precipitation (TPre) ($p < 0.05$). Panels (A) and (B) represent nighttime and midday conditions,
 398 respectively. For each predictor, “-O” denotes the OLS standardized coefficient, “-R” the ridge
 399 regression coefficient, and “-P” the partial correlation coefficient. Model skill was evaluated using
 400 the coefficients of determination derived from both OLS ($R^2_{(OLS)}$) and ridge regression ($R^2_{(ridge)}$).

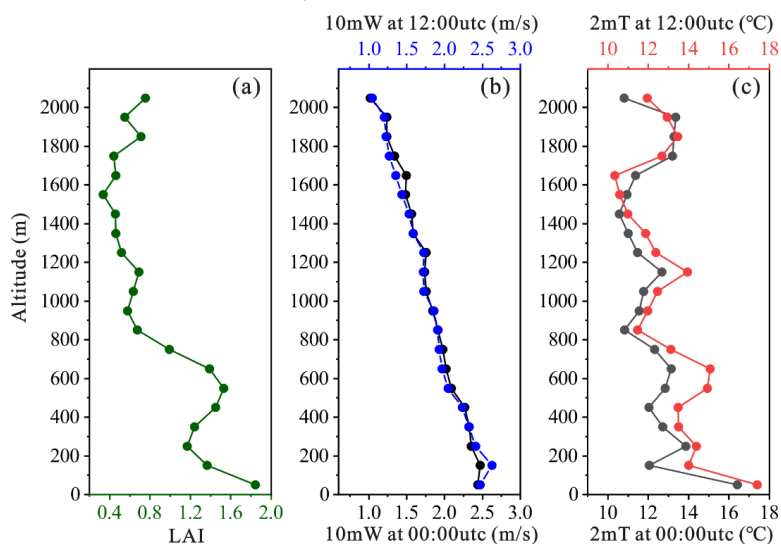


401 Air temperature, closely linked to climate change, influences fire activity by
402 modulating fuel drying and convective processes (Dastour et al., 2024; Duane et al.,
403 2021). However, temperature exhibited negligible effects, with both OLS and ridge
404 coefficients remaining close to zero across all elevations under both nighttime and
405 midday conditions. The weak elevational dependence of 2 m air temperature (Figure 7)
406 suggests that temperature alone cannot explain the observed decline in fire occurrence.
407 At mid-elevations, nighttime temperature exhibits a weak negative partial correlation
408 with fire occurrence, while daytime temperature shows a positive association,
409 highlighting the complex and diurnally dependent influence of temperature under
410 topographic constraints. In contrast, precipitation emerges as a robust suppressor of fire
411 activity across all elevation bands, with the strongest effects observed at mid-elevations.
412 The consistently negative regression coefficients indicate that precipitation deficits are
413 a primary determinant of fire occurrence and spatial distribution, consistent with
414 previous findings linking fire activity to precipitation amount and rainy-day frequency
415 (Kim et al., 2025). Relative humidity likely reinforces this effect by further modulating
416 fuel moisture, particularly in boreal forest systems (Veraverbeke et al., 2017; Dastour
417 et al., 2024).

418 Wind speed also exhibits strong elevational dependence. Nighttime wind speed
419 shows a positive association with fire occurrence below 1800 m in both OLS and ridge
420 models, with the strongest influence at mid-elevations (Figure 6). Daytime wind speed
421 is positively related to fire activity at low elevations but shows no significant
422 relationship at mid-elevations, likely reflecting differences between daytime up-valley
423 winds and nighttime downslope flows. In mountainous terrain, downslope flows may
424 advect warm and dry air toward lower elevations, creating fire-favorable conditions
425 when fuels are sufficiently dry (Abatzoglou et al., 2023; Abatzoglou et al., 2021).
426 Partial correlation analyses indicate that, when isolated from other factors, wind speed
427 remains positively associated with fire activity across elevations below 2000 m,
428 particularly at mid-elevations. Elevated wind speeds enhance fire activity by increasing
429 evaporative drying, promoting sustained combustion, and facilitating ember transport



430 (Ma et al., 2020; Jones et al., 2022).



431

432 Figure 7. Elevational patterns of multiyear mean variables. (a) Leaf area index (LAI). (b) 10 m wind
433 speed (10mW) at 00:00 and 12:00 utc. (c) 2 m air temperature (2mT) at 00:00 utc and 12:00 utc.

434 Together, these results identify precipitation, wind speed, and vegetation
435 abundance as primary drivers of the elevation-dependent distribution of forest fires. At
436 mid-elevations, fire activity is jointly controlled by sufficient fuel availability and
437 aridity, the latter mediated by reduced precipitation and elevation-specific wind regimes.
438 In addition, enhanced FAOD associated with fire-emitted smoke aerosols—dominated
439 by light-absorbing black carbon (Yu et al., 2019)—may further contribute to
440 atmospheric heating and fuel drying at seasonal to interannual timescales (Pei et al.,
441 2025), potentially reinforcing fire-favorable conditions. Several potentially important
442 drivers, including anthropogenic ignitions, lightning frequency, soil moisture, and
443 regional fire management practices, were not explicitly considered in this analysis. In
444 addition, the limited number of grid cells (< 10) between 1300 and 2100 m reduces
445 statistical robustness, suggesting that fire controls at these elevations may be more
446 complex at the global scale. These unaccounted factors likely contribute to the residual
447 variability in fire occurrence and warrant further investigation.

448 4. Conclusion

449 Across global forested regions from 2012 to 2024, we analyze spatiotemporal



450 variability in forest fire activity and its associated AOD, together with their elevation-
451 dependent drivers, across global forested regions during 2012–2024. Satellite
452 observations reveal a modest but statistically significant increase in forest fire
453 occurrence, with a global mean linear trend of $+2.89 \text{ \% yr}^{-1}$. Fire trends vary
454 substantially among forest types, with ENF exhibiting the strongest positive trends,
455 while DNF and MF show no significant changes. Fire-associated aerosol loading is
456 dominated by fine-mode particles. The consistent positive trends and statistically
457 significant relationships between FAOD and fire pixel counts, together with the absence
458 of a corresponding response in CAOD, indicate that forest fire emissions primarily
459 enhance the fine aerosol fraction. Both the multiyear mean fire pixel counts and its
460 temporal trend decline systematically with increasing elevation, from lowlands to
461 elevations above 2000 m, highlighting a pronounced elevational control on global forest
462 fire activity. In contrast, FAOD exhibits a more complex elevational structure. Below
463 600 m, FAOD trends broadly track fire occurrence, whereas at mid-elevations (600–
464 1400 m) FAOD displays elevated mean values and increasing trends despite declining
465 fire occurrence. This divergence suggests that mid-elevation aerosol burdens are
466 influenced not only by local fire activity but also by shifts in forest-type composition
467 and by topographically modulated smoke transport, including aerosol self-lifting driven
468 by radiative absorption and atmospheric convection.

469 Elevation-stratified multiple linear regression analyses further indicate that forest
470 fire activity is primarily controlled by the combined effects of fuel availability and
471 aridity. Fuel load, represented by leaf area index, plays a critical role at mid-elevations,
472 while precipitation consistently exerts a suppressive influence on fire occurrence across
473 all elevation bands. Wind speed emerges as an important contributor to fuel drying and
474 fire spread, especially in mid-elevation regions. In contrast, temperature and the FWI
475 show limited independent explanatory power once elevation and other covarying
476 factors are considered. Overall, these results highlight elevation as an important
477 organizing dimension linking forest fire activity, aerosol emissions, and their
478 underlying drivers at the global scale. By elucidating how fuel characteristics,



479 meteorological conditions, and topography jointly regulate fire–aerosol interactions
480 across elevation gradients, this study provides a physically grounded framework for
481 improving wildfire risk assessment, interpreting fire-driven aerosol impacts, and
482 refining fire management strategies under a changing climate. Continued investigation
483 incorporating anthropogenic ignitions, lightning activity, and region-specific
484 management practices will be essential for further constraining elevation-dependent
485 fire regimes.

486

487 **Data availability**

488 Active fire detections at 375 m resolution were obtained from the NASA Land-SIPS
489 VIIRS product, provided through the Fire Information for Resource Management
490 System (FIRMS) (<https://earthdata.nasa.gov/firms>). Elevation information was derived
491 from the 2024 General Bathymetric Chart of the Oceans (GEBCO) global gridded
492 dataset (doi:10.5285/1c44ce99-0a0d-5f4f-e063-7086abc0ea0f), available at
493 <https://www.gebco.net/>. Land cover classifications were taken from the MODIS Land
494 Cover Type Yearly Climate Modeling Grid (CMG; MCD12Q1), distributed via the
495 Level-1 and Atmosphere Archive & Distribution System (LAADS DAAC)
496 (<https://ladsweb.modaps.eosdis.nasa.gov/search/order/1>). Historical Fire Weather
497 Index (FWI) data were sourced from the Copernicus Emergency Management Service
498 (<https://doi.org/10.24381/cds.0e89c522>). Meteorological variables and leaf area index
499 (LAI) were extracted from the ECMWF Reanalysis v5 (ERA5) archive
500 (<https://cds.climate.copernicus.eu/datasets>). The daily global FAOD and CAOD
501 datasets at 500 nm are available from the authors upon request.

502

503 **Author contributions**

504 CZ initiated and supervised the study. QP carried out the data analysis and drafted the
505 initial manuscript. XY contributed the daily global FAOD and CAOD datasets. All
506 authors (CZ, QP, XY, XY, AC, and XW) participated in improving the manuscript.

507

508 **Competing interests**

509 The authors declare that they have no conflict of interest.

510

511 **Acknowledgments**

512 This work is supported by the Yunnan Provincial Science and Technology Project at
513 Southwest United Graduate School (grant number 202302AP370003). We are deeply



514 appreciative of MODIS, GEBCO, ECMWF and NASA's FIRMS teams for granting
515 access to their valuable data.

516

517 **References**

- 518 Abatzoglou, J. T. and Williams, A. P.: Impact of anthropogenic climate change on wildfire across western
519 US forests, *P Natl Acad Sci USA*, 113, 11770-11775, 10.1073/pnas.1607171113, 2016.
- 520 Abatzoglou, J. T., Rupp, D. E., O'Neill, L. W., and Sadegh, M.: Compound Extremes Drive the Western
521 Oregon Wildfires of September 2020, *Geophysical Research Letters*, 48, e2021GL092520, ARTN
522 e2021GL09252010.1029/2021GL092520, 2021.
- 523 Abatzoglou, J. T., Kolden, C. A., Williams, A. P., Sadegh, M., Balch, J. K., and Hall, A.: Downslope
524 Wind-Driven Fires in the Western United States, *Earths Future*, 11, e2022EF003471, ARTN
525 e2022EF00347110.1029/2022EF003471, 2023.
- 526 Abatzoglou, J. T., Kolden, C. A., Cullen, A. C., Sadegh, M., Williams, E. L., Turco, M., and Jones, M.
527 W.: Climate change has increased the odds of extreme regional forest fire years globally, *Nature*
528 *Communications*, 16, 6390, ARTN 639010.1038/s41467-025-61608-1, 2025.
- 529 Alexander, M. E. and Cruz, M. G.: Crown fire dynamics in conifer forests, in: *Synthesis of Knowledge*
530 *of Extreme Fire Behavior*, 107-142, 2011.
- 531 Andela, N., Morton, D. C., Giglio, L., Chen, Y., van der Werf, G. R., Kasibhatla, P. S., DeFries, R. S.,
532 Collatz, G. J., Hantson, S., Kloster, S., Bachelet, D., Forrest, M., Lasslop, G., Li, F., Mangeon, S.,
533 Melton, J. R., Yue, C., and Randerson, J. T.: A human-driven decline in global burned area, *Science*,
534 356, 1356-1361, 10.1126/science.aal4108, 2017.
- 535 Andreae, M. O., Rosenfeld, D., Artaxo, P., Costa, A. A., Frank, G. P., Longo, K. M., and Silva-Dias, M.
536 A. F.: Smoking rain clouds over the Amazon, *Science*, 303, 1337-1342, DOI
537 10.1126/science.1092779, 2004.
- 538 Baek, S., Lim, J., and Kim, W.: Analysis on the Fire Progression and Severity Variation of the Massive
539 Forest Fire Occurred in Uljin, Korea, 2022, *Forests*, 13, 2185, ARTN 218510.3390/f13122185, 2022.
- 540 Birch, D. S., Morgan, P., Kolden, C. A., Abatzoglou, J. T., Dillon, G. K., Hudak, A. T., and Smith, A. M.
541 S.: Vegetation, topography and daily weather influenced burn severity in central Idaho and western
542 Montana forests, *Ecosphere*, 6, art17, ArtN 1710.1890/Es14-00213.1, 2015.
- 543 Blanchard-Wrigglesworth, E., DeRepentigny, P., and Frierson, D. M. W.: Increasing boreal fires reduce
544 future global warming and sea ice loss, *Proceedings of the National Academy of Sciences*, 122,
545 e2424614122, 10.1073/pnas.2424614122, 2025.
- 546 Bowman, D. M. J. S., Balch, J. K., Artaxo, P., Bond, W. J., Carlson, J. M., Cochrane, M. A., D'Antonio,
547 C. M., DeFries, R. S., Doyle, J. C., Harrison, S. P., Johnston, F. H., Keeley, J. E., Krawchuk, M. A.,
548 Kull, C. A., Marston, J. B., Moritz, M. A., Prentice, I. C., Roos, C. I., Scott, A. C., Swetnam, T. W.,
549 van der Werf, G. R., and Pyne, S. J.: Fire in the Earth System, *Science*, 324, 481-484,
550 10.1126/science.1163886, 2009.
- 551 Canadell, J. G., Meyer, C. P., Cook, G. D., Dowdy, A., Briggs, P. R., Knauer, J., Pepler, A., and Haverd,
552 V.: Multi-decadal increase of forest burned area in Australia is linked to climate change, *Nature*
553 *Communications*, 12, 6921, ARTN 692110.1038/s41467-021-27225-4, 2021.
- 554 Chen, J. Y., Chen, H. W., Li, Z. Q., Wang, Q., Wang, G. Q., Jia, K., and Yan, X.: Divergent radiative
555 forcing of fine-mode aerosols across tree genera during wildfires in North America and Europe,



- 556 Journal of Hazardous Materials, 495, 138881, ARTN 13888110.1016/j.jhazmat.2025.138881, 2025.
- 557 Clarke, H., Di Giuseppe, F., Johnston, L., Marlon, J., Penman, T., Pitman, A. J., van der Werf, G. R., and
558 Flannigan, M. D.: Gazing into the flames: A guide to assessing the impacts of climate change on
559 landscape fire, *Science Advances*, 11, eadz2429, ARTN eadz242910.1126/sciadv.adz2429, 2025.
- 560 Cunningham, C. X., Williamson, G. J., and Bowman, D. M. J. S.: Increasing frequency and intensity of
561 the most extreme wildfires on Earth, *Nature Ecology & Evolution*, 8, 1420-1425, 10.1038/s41559-
562 024-02452-2, 2024.
- 563 Dastour, H., Ahmed, M. R., and Hassan, Q. K.: Analysis of forest fire patterns and their relationship with
564 climate variables in Alberta's natural subregions, *Ecological Informatics*, 80, 102531, ARTN
565 10253110.1016/j.ecoinf.2024.102531, 2024.
- 566 de Laat, A. T. J., Stein Zweers, D. C., Boers, R., and Tuinder, O. N. E.: A solar escalator: Observational
567 evidence of the self-lifting of smoke and aerosols by absorption of solar radiation in the February
568 2009 Australian Black Saturday plume, *Journal of Geophysical Research: Atmospheres*, 117,
569 10.1029/2011jd017016, 2012.
- 570 Duane, A., Castellnou, M., and Brotons, L.: Towards a comprehensive look at global drivers of novel
571 extreme wildfire events, *Climatic Change*, 165, 43, ARTN 4310.1007/s10584-021-03066-4, 2021.
- 572 Fan, H., Wang, Y., Zhao, C. F., Yang, Y. K., Yang, X. C., Sun, Y., and Jiang, S. Y.: The Role of Primary
573 Emission and Transboundary Transport in the Air Quality Changes During and After the COVID-
574 19 Lockdown in China, *Geophysical Research Letters*, 48, e2020GL091065, ARTN
575 e2020GL09106510.1029/2020GL091065, 2021.
- 576 Gatti, L. V., Basso, L. S., Miller, J. B., Gloor, M., Domingues, L. G., Cassol, H. L. G., Tejada, G., Aragao,
577 L. E. O. C., Nobre, C., Peters, W., Marani, L., Arai, E., Sanches, A. H., Corrêa, S. M., Anderson, L.,
578 Von Randow, C., Correia, C. S. C., Crispim, S. P., and Neves, R. A. L.: Amazonia as a carbon source
579 linked to deforestation and climate change, *Nature*, 595, 388-+, 10.1038/s41586-021-03629-6, 2021.
- 580 Hamilton, D. S., Perron, M. M. G., Bond, T. C., Bowie, A. R., Buchholz, R. R., Guieu, C., Ito, A.,
581 Maenhaut, W., Myriokefalitakis, S., Olgun, N., Rathod, S. D., Schepanski, K., Tagliabue, A.,
582 Wagner, R., and Mahowald, N. M.: Earth, Wind, Fire, and Pollution: Aerosol Nutrient Sources and
583 Impacts on Ocean Biogeochemistry, *Annual Review of Marine Science*, 14, 303-330,
584 10.1146/annurev-marine-031921-013612, 2022.
- 585 Harper, H. and Sandwell, D. T.: Global Predicted Bathymetry Using Neural Networks, *Earth and Space
586 Science*, 11, e2023EA003199, ARTN e2023EA00319910.1029/2023EA003199, 2024.
- 587 Huang, Y. H., Jin, Y. F., Schwartz, M. W., and Thorne, J. H.: Intensified burn severity in California's
588 northern coastal mountains by drier climatic condition, *Environmental Research Letters*, 15, 104033,
589 ARTN 10403310.1088/1748-9326/aba6af, 2020.
- 590 Jolly, W. M., Cochrane, M. A., Freeborn, P. H., Holden, Z. A., Brown, T. J., Williamson, G. J., and
591 Bowman, D. M. J. S.: Climate-induced variations in global wildfire danger from 1979 to 2013,
592 *Nature Communications*, 6, 7537, 10.1038/ncomms8537, 2015.
- 593 Jones, M. W., Veraverbeke, S., Andela, N., Doerr, S. H., Kolden, C., Mataveli, G., Pettinari, M. L., Le
594 Quéré, C., Rosan, T. M., van der Werf, G. R., van Wees, D., and Abatzoglou, J. T.: Global rise in
595 forest fire emissions linked to climate change in the extratropics, *Science*, 386, ARTN
596 eadl588910.1126/science.adl5889, 2024.
- 597 Jones, M. W., Abatzoglou, J. T., Veraverbeke, S., Andela, N., Lasslop, G., Forkel, M., Smith, A. J. P.,
598 Burton, C., Betts, R. A., van der Werf, G. R., Sitch, S., Canadell, J. G., Santin, C., Kolden, C., Doerr,



- 599 S. H., and Le Quéré, C.: Global and Regional Trends and Drivers of Fire Under Climate Change,
600 *Reviews of Geophysics*, 60, e2020RG000726, ARTN e2020RG00072610.1029/2020RG000726,
601 2022.
- 602 Kaskaoutis, D. G., Kumar, S., Sharma, D., Singh, R. P., Kharol, S. K., Sharma, M., Singh, A. K., Singh,
603 S., Singh, A., and Singh, D.: Effects of crop residue burning on aerosol properties, plume
604 characteristics, and long-range transport over northern India, *J Geophys Res-Atmos*, 119, 5424-
605 5444, 10.1002/2013jd021357, 2014.
- 606 Keywood, M., Kanakidou, M., Stohl, A., Dentener, F., Grassi, G., Meyer, C. P., Torseth, K., Edwards, D.,
607 Thompson, A. M., Lohmann, U., and Burrows, J.: Fire in the Air: Biomass Burning Impacts in a
608 Changing Climate, *Critical Reviews in Environmental Science and Technology*, 43, 40-83,
609 10.1080/10643389.2011.604248, 2013.
- 610 Kim, J., Kim, T., Lee, Y. E., and Im, S.: Spatial and temporal variability of forest fires in the Republic of
611 Korea over 1991-2020, *Natural Hazards*, 121, 9801-9821, 10.1007/s11069-025-07169-4, 2025.
- 612 Kirchmeier-Young, M. C., Malinina, E., Barber, Q. E., Perdomo, K. G., Curasi, S. R., Liang, Y. X., Jain,
613 P., Gillett, N. P., Parisien, M. A., Cannon, A. J., Lima, A. R., Arora, V. K., Boulanger, Y., Melton, J.
614 R., Van Vliet, L., and Zhang, X. B.: Human driven climate change increased the likelihood of the
615 2023 record area burned in Canada, *Npj Climate and Atmospheric Science*, 7, 316, ARTN
616 31610.1038/s41612-024-00841-9, 2024.
- 617 Koren, I., Kaufman, Y. J., Remer, L. A., and Martins, J. V.: Measurement of the effect of Amazon smoke
618 on inhibition of cloud formation, *Science*, 303, 1342-1345, DOI 10.1126/science.1089424, 2004.
- 619 Kumar, S. and Kumar, A.: Hotspot and trend analysis of forest fires and its relation to climatic factors in
620 the western Himalayas, *Natural Hazards*, 114, 3529-3544, 10.1007/s11069-022-05530-5, 2022.
- 621 Lapola, D. M., Pinho, P., Barlow, J., Aragao, L. E. O. C., Berenguer, E., Carmenta, R., Liddy, H. M.,
622 Seixas, H., Silva, C. V. J., Silva-Junior, C. H. L., Alencar, A. A. C., Anderson, L. O., Armenteras,
623 D., Brovkin, V., Calders, K., Chambers, J., Chini, L., Costa, M. H., Faria, B. L., Fearnside, P. M.,
624 Ferreira, J., Gatti, L., Gutierrez-Velez, V. H., Han, Z. G., Hibbard, K., Koven, C., Lawrence, P.,
625 Pongratz, J., Portela, B. T. T., Rounsevell, M., Ruane, A. C., Schaldach, R., da Silva, S. S., von
626 Randow, C., and Walker, W. S.: The drivers and impacts of Amazon forest degradation, *Science*,
627 379, 349-+, ARTN eabp862210.1126/science.abp8622, 2023.
- 628 Lau, K. M., Kim, M. K., and Kim, K. M.: Asian summer monsoon anomalies induced by aerosol direct
629 forcing: the role of the Tibetan Plateau, *Climate Dynamics*, 26, 855-864, 10.1007/s00382-006-0114-
630 z, 2006.
- 631 Liu, G. Y., Li, J., Ying, T., Su, H. X., Huang, X., and Yu, Y.: Increasing Fire Weather Potential Over
632 Northeast China Linked to Declining Bering Sea Ice, *Geophysical Research Letters*, 50,
633 e2023GL105931, ARTN e2023GL10593110.1029/2023GL105931, 2023.
- 634 Luo, N. A., Zhang, Y., Jiang, Y. Z., Zuo, C., Chen, J. Y., Zhao, W. J., Shi, W. Z., and Yan, X.: Unveiling
635 global land fine- and coarse-mode aerosol dynamics from 2005 to 2020 using enhanced satellite-
636 based monthly inversion data, *Environmental Pollution*, 348, 123838, ARTN
637 12383810.1016/j.envpol.2024.123838, 2024.
- 638 Ma, Q. H., Wei, L. Y., Wang, Y., Zhang, G. J., Zhou, X. L., and Wang, B.: Fire heat affects the impacts
639 of wildfires on air pollution in the United States, *Science*, 389, 1137-1142, 10.1126/science.ads1957,
640 2025.
- 641 Ma, W., Feng, Z., Cheng, Z., Chen, S., and Wang, F.: Identifying Forest Fire Driving Factors and Related



- 642 Impacts in China Using Random Forest Algorithm, 10.3390/fl1050507, 2020.
- 643 Menon, S., Hansen, J., Nazarenko, L., and Luo, Y. F.: Climate effects of black carbon aerosols in China
644 and India, *Science*, 297, 2250-2253, DOI 10.1126/science.1075159, 2002.
- 645 Ohneiser, K., Ansmann, A., Witthuhn, J., Deneke, H., Chudnovsky, A., Walter, G., and Senf, F.: Self-
646 lofting of wildfire smoke in the troposphere and stratosphere: simulations and space lidar
647 observations, *Atmospheric Chemistry and Physics*, 23, 2901-2925, 10.5194/acp-23-2901-2023,
648 2023.
- 649 Pan, Y. D., Birdsey, R. A., Fang, J. Y., Houghton, R., Kauppi, P. E., Kurz, W. A., Phillips, O. L., Shvidenko,
650 A., Lewis, S. L., Canadell, J. G., Ciais, P., Jackson, R. B., Pacala, S. W., McGuire, A. D., Piao, S.
651 L., Rautiainen, A., Sitch, S., and Hayes, D.: A Large and Persistent Carbon Sink in the World's
652 Forests, *Science*, 333, 988-993, 10.1126/science.1201609, 2011.
- 653 Parisien, M. A., Barber, Q. E., Bourbonnais, M. L., Daniels, L. D., Flannigan, M. D., Gray, R. W.,
654 Hoffman, K. M., Jain, P., Stephens, S. L., Taylor, S. W., and Whitman, E.: Abrupt, climate-induced
655 increase in wildfires in British Columbia since the mid-2000s, *Communications Earth &
656 Environment*, 4, ARTN 30910.1038/s43247-023-00977-1, 2023.
- 657 Parks, S. A., Holsinger, L. M., Panunto, M. H., Jolly, W. M., Dobrowski, S. Z., and Dillon, G. K.: High-
658 severity fire: evaluating its key drivers and mapping its probability across western US forests,
659 *Environmental Research Letters*, 13, 044037, ARTN 04403710.1088/1748-9326/aab791, 2018.
- 660 Pei, Q. M., Zhao, C. F., Yang, Y. K., Chen, A. N., Cong, Z. Y., Wan, X., Zhang, H. T., and Wu, G. M.:
661 Wildfires heat the middle troposphere over the Himalayas and Tibetan Plateau during the peak of
662 fire season, *Atmospheric Chemistry and Physics*, 25, 10443-10456, 10.5194/acp-25-10443-2025,
663 2025.
- 664 Qian, Y.: Burning questions on wildfire, *Science*, 389, 1086-1087, 10.1126/science.aea7430, 2025.
- 665 Rogeau, M. P. and Armstrong, G. W.: Quantifying the effect of elevation and aspect on fire return
666 intervals in the Canadian Rocky Mountains, *Forest Ecology and Management*, 384, 248-261,
667 10.1016/j.foreco.2016.10.035, 2017.
- 668 Sharples, J. J., Mills, G. A., and McRae, R. H. D.: Extreme drying events in the Australian high-country
669 and their implications for bushfire risk management, *Australian Meteorological and Oceanographic
670 Journal*, 62, 157-169, 10.22499/2.6203.004, 2012.
- 671 Su, H. X., Yu, Y., Guo, W. D., and Mao, J. F.: Convective potential and fuel availability complement
672 near-surface weather in regulating global wildfire activity, *Science Advances*, 11, eadp7765, ARTN
673 eadp776510.1126/sciadv.adp7765, 2025.
- 674 Tang, W. Y., Llort, J., Weis, J., Perron, M. M. G., Basart, S., Li, Z. C., Sathyendranath, S., Jackson, T.,
675 Rodriguez, E. S., Proemse, B. C., Bowie, A. R., Schallenberg, C., Strutton, P. G., Matear, R., and
676 Cassar, N.: Widespread phytoplankton blooms triggered by 2019-2020 Australian wildfires, *Nature*,
677 597, 370+, 10.1038/s41586-021-03805-8, 2021.
- 678 Tian, X. R., Zhao, F. J., Shu, L. F., and Wang, M. Y.: Distribution characteristics and the influence factors
679 of forest fires in China, *Forest Ecology and Management*, 310, 460-467,
680 10.1016/j.foreco.2013.08.025, 2013.
- 681 Van Wagner, C. E.: Development and structure of the Canadian Forest Fire Weather Index System.
682 Canadian Forestry Service, Headquarters, Ottawa, 1987.
- 683 Veraverbeke, S., Rogers, B. M., Goulden, M. L., Jandt, R. R., Miller, C. E., Wiggins, E. B., and Randerson,
684 J. T.: Lightning as a major driver of recent large fire years in North American boreal forests, *Nature*



- 685 Climate Change, 7, 529+, 10.1038/Nclimate3329, 2017.
- 686 Walker, X. J., Rogers, B. M., Veraverbeke, S., Johnstone, J. F., Baltzer, J. L., Barrett, K., Bourgeau-
687 Chavez, L., Day, N. J., de Groot, W. J., Dieleman, C. M., Goetz, S., Hoy, E., Jenkins, L. K., Kane,
688 E. S., Parisien, M. A., Potter, S., Schuur, E. A. G., Turetsky, M., Whitman, E., and Mack, M. C.:
689 Fuel availability not fire weather controls boreal wildfire severity and carbon emissions, *Nature*
690 *Climate Change*, 10, 1130-1136, 10.1038/s41558-020-00920-8, 2020.
- 691 Wang, B., Spessa, A. C., Feng, P. Y., Hou, X., Yue, C., Luo, J. J., Ciais, P., Waters, C., Cowie, A., Nolan,
692 R. H., Nikonovas, T., Jin, H. D., Walshaw, H., Wei, J. H., Guo, X. W., Liu, D. L., and Yu, Q.: Extreme
693 fire weather is the major driver of severe bushfires in southeast Australia, *Science Bulletin*, 67, 655-
694 664, 10.1016/j.scib.2021.10.001, 2022a.
- 695 Wang, H., Jin, B., Zhang, K., Aktar, S., and Song, Z.: Effectiveness in Mitigating Forest Fire Ignition
696 Sources: A Statistical Study Based on Fire Occurrence Data in China, 10.3390/fire5060215,
697 2022b.
- 698 Wang, W. W., Wang, X. L., Wu, W. L., Guo, F. T., Park, J. N., and Wang, G. Y.: Burn Severity in Canada's
699 Mountain National Parks: Patterns, Drivers, and Predictions, *Geophysical Research Letters*, 49,
700 ARTN e2022GL09794510.1029/2022GL097945, 2022c.
- 701 Wang, W. W., Wang, X. L., Flannigan, M. D., Guindon, L., Swystun, T., Castellanos-Acuna, D., Wu, W.
702 L., and Wang, G. Y.: Canadian forests are more conducive to high-severity fires in recent decades,
703 *Science*, 387, 91+, 10.1126/science.ado1006, 2025.
- 704 Ward, M., Tulloch, A. I. T., Radford, J. Q., Williams, B. A., Reside, A. E., Macdonald, S. L., Mayfield,
705 H. J., Maron, M., Possingham, H. P., Vine, S. J., O'Connor, J. L., Massingham, E. J., Greenville, A.
706 C., Woinarski, J. C. Z., Garnett, S. T., Lintermans, M., Scheele, B., Carwardine, J., Nimmo, D. G.,
707 Lindenmayer, D. B., Kooyman, R. M., Simmonds, J. S., Sonter, L. J., and Watson, J. E. M.: Impact
708 of 2019-2020 mega-fires on Australian fauna habitat, *Nature Ecology & Evolution*, 4, 1321+,
709 10.1038/s41559-020-1251-1, 2020.
- 710 Whitman, E., Parisien, M. A., Thompson, D. K., Hall, R. J., Skakun, R. S., and Flannigan, M. D.:
711 Variability and drivers of burn severity in the northwestern Canadian boreal forest, *Ecosphere*, 9,
712 e02128, ARTN e0212810.1002/ecs2.2128, 2018.
- 713 Xu, R., Yu, Y., Meng, X. L., Xue, H. W., Zhao, C. F., and Lin, J. T.: Atmospheric Convection and Aerosol
714 Absorption Boost Wildfire Smoke Injection, *Geophysical Research Letters*, 52, e2025GL115989,
715 ARTN e2025GL11598910.1029/2025GL115989, 2025.
- 716 Yan, X., Zuo, C., Li, Z. Q., Chen, H. W., Jiang, Y. Z., Wang, Q., Wang, G. Q., Jia, K., Yinglan, A., Chen,
717 Z. Y., and Chen, J. Y.: Substantial Underestimation of Fine-Mode Aerosol Loading from Wildfires
718 and Its Radiative Effects in Current Satellite-Based Retrievals over the United States,
719 *Environmental Science & Technology*, 58, 15661-15671, 10.1021/acs.est.4c02498, 2024.
- 720 Yang, X., Wang, Y., Zhao, C., Fan, H., Yang, Y., Chi, Y., Shen, L., and Yan, X.: Health risk and disease
721 burden attributable to long-term global fine-mode particles, *Chemosphere*, 287, 132435,
722 10.1016/j.chemosphere.2021.132435, 2022.
- 723 Yang, X. C., Zhao, C. F., Yang, Y. K., and Fan, H.: Long-term multi-source data analysis about the
724 characteristics of aerosol optical properties and types over Australia, *Atmospheric Chemistry and*
725 *Physics*, 21, 3803-3825, 10.5194/acp-21-3803-2021, 2021a.
- 726 Yang, X. C., Zhao, C. F., Yang, Y. K., Yan, X., and Fan, H.: Statistical aerosol properties associated with
727 fire events from 2002 to 2019 and a case analysis in 2019 over Australia, *Atmospheric Chemistry*



728 and Physics, 21, 3833-3853, 10.5194/acp-21-3833-2021, 2021b.
729 Yang, X. C., Zhao, C. F., Zhao, W. J., Fan, H., and Yang, Y. K.: Characterization of global fire activity
730 and its spatiotemporal patterns for different land cover types from 2001 to 2020, *Environmental*
731 *Research*, 227, 115746, ARTN 11574610.1016/j.envres.2023.115746, 2023.
732 Yu, P. F., Toon, O. B., Bardeen, C. G., Zhu, Y. Q., Rosenlof, K. H., Portmann, R. W., Thornberry, T. D.,
733 Gao, R. S., Davis, S. M., Wolf, E. T., de Gouw, J., Peterson, D. A., Fromm, M. D., and Robock, A.:
734 Black carbon lofts wildfire smoke high into the stratosphere to form a persistent plume, *Science*,
735 365, 587-590, 10.1126/science.aax1748, 2019.
736 Yu, Y. and Ginoux, P.: Enhanced dust emission following large wildfires due to vegetation disturbance,
737 *Nature Geoscience*, 15, 878-+, 10.1038/s41561-022-01046-6, 2022.
738 Yu, Y., Mao, J. F., Thornton, P. E., Notaro, M., Wullschleger, S. D., Shi, X. Y., Hoffman, F. M., and Wang,
739 Y. P.: Quantifying the drivers and predictability of seasonal changes in African fire, *Nature*
740 *Communications*, 11, 10.1038/s41467-020-16692-w, 2020.
741 Zhang, Q., Wang, Y. X. Z., Xiao, Q. Y., Geng, G. N., Davis, S. J., Liu, X. D., Yang, J., Liu, J. J., Huang,
742 W. Y., He, C. P., Luo, B. H., Martin, R. V., Brauer, M., Randerson, J. T., and He, K. B.: Long-range
743 PM pollution and health impacts from the 2023 Canadian wildfires, *Nature*, 645, 672-678,
744 10.1038/s41586-025-09482-1, 2025.
745 Zhao, J., Yue, C., Wang, J., Hantson, S., Wang, X., He, B., Li, G., Wang, L., Zhao, H., and Luyssaert, S.:
746 Forest fire size amplifies postfire land surface warming, *Nature*, 633, 828-834, 10.1038/s41586-
747 024-07918-8, 2024.
748 Zheng, B., Ciais, P., Chevallier, F., Chuvieco, E., Chen, Y., and Yang, H.: Increasing forest fire emissions
749 despite the decline in global burned area, *Science Advances*, 7, eabh2646, ARTN
750 eabh264610.1126/sciadv.abh2646, 2021.
751